THE JOURNAL OF CHEMICAL PHYSICS **130**, 114907 (2009)

Multiscale modeling of lamellar mesophases

V. Kumaran,[a] Y. K. V. V. N. Krishna Babu, and J. Sivaramakrishna
Department of Chemical Engineering, Indian Institute of Science, Bangalore 560 012, India

(Received 30 September 2008; accepted 4 December 2008; published online 19 March 2009)

The mesoscale simulation of a lamellar mesophase based on a free energy functional is examined with the objective of determining the relationship between the parameters in the model and molecular parameters. Attention is restricted to a symmetric lamellar phase with equal volumes of hydrophilic and hydrophobic components. Apart from the lamellar spacing, there are two parameters in the free energy functional. One of the parameters, r, determines the sharpness of the interface, and it is shown how this parameter can be obtained from the interface profile in a molecular simulation. The other parameter, A, provides an energy scale. Analytical expressions are derived to relate these parameters to r and A to the bending and compression moduli and the permeation constant in the macroscopic equation to the Onsager coefficient in the concentration diffusion equation. The linear hydrodynamic response predicted by the theory is verified by carrying out a mesoscale simulation using the lattice-Boltzmann technique and verifying that the analytical predictions are in agreement with simulation results. A macroscale model based on the layer thickness field and the layer normal field is proposed, and the relationship between the parameters in the macroscale model from the parameters in the mesoscale free energy functional is obtained. © *2009 American Institute of Physics*. [DOI: 10.1063/1.3077004]

I. INTRODUCTION

Many industrial applications involve the transport and processing of surfactant solutions. Depending on the relative concentrations of water, oil, and surfactants, these self-assemble into micelles, lamellar, or hexagonal phases. In order to design process equipment, it is necessary to accurately predict the flow behavior accurately. However, lamellar and hexagonal phases exhibit complex rheological behavior because they are anisotropic fluids.[1] A perfectly aligned lamellar phase, for example, exhibits fluidlike behavior when the normal to the lamellae is along the shear or vorticity direction, but has a solidlike resistance to flow when the normal is along the flow direction. In addition, even though a perfect defect-free stack of layers is the final equilibrium state, real samples are rarely defect-free due to kinetic constraints. For these reasons, isotropic non-Newtonian constitutive equations[2] are not sufficient for these systems, and it is necessary to include additional fields (such as the unit normal to the layers) to accurately describe their rheology. Moreover, shear treatment alters the structure of the lamellar phase, and this in turn affects the rheology. The lamellar spacing is typically small compared to macroscopic scales (the distance between layers in lyotropic liquid crystalline phases is usually a few hundred angstroms), and so a macroscopic simulation which resolves details on the length scale of the lamellar spacing is unrealistic. Since the rheology of the liquid depends on structure, it is difficult to obtain closed form equations for the density and momentum fields alone in these systems.

The lamellar spacing in lyotropic liquid crystals is 10–100 Å, and a typical macroscopic sample contains 10^8 to 10^{12} lamellae. Therefore, it is not possible to simulate flows in macroscopic systems using this technique. It is necessary to use different simulation techniques (molecular, mesoscale, macroscale) for different lengths and time scales. The molecular dynamics simulations typically resolve the positions and momenta of all the atoms in an atomistic simulation or those of a group of atoms in coarse-grained or united atom simulations. It is computationally infeasible to simulate more than a single bilayer using these simulation techniques. For a mesoscale simulation which resolves a few lamellae, mesoscale techniques have been developed.[3–7] These simulations typically deal with a concentration (order-parameter) field which is the difference in the concentrations of the hydrophilic and hydrophobic species. It is possible to carry out simulations of a few tens of lamellae with mesoscale technique, but the sample size is still small compared to samples that encountered in practical applications, which are millimeters or centimeters in size. At the macroscale, it is necessary to use simulations where only continuum variables such as the density and velocity fields are retained. The progression in the hierarchy from the molecular to the macroscale involves a coarse-graining procedure, where only the necessary information from the smaller scale simulation is passed on to the larger scale simulation. In order to be able to make quantitative calculations, it is essential to have a procedure for calculating the parameters in the larger scale simulation from those in the smaller scale simulation. This relationship between the parameters in simulations at different scales for a lamellar mesophase is the subject of the present analysis.

The mesoscale model used here is based on a free energy functional, which is chosen so that a lamellar phase is obtained as the solution by minimizing the free energy. The order parameter used here is a concentration field ψ which is

---

[a] Electronic mail: kumaran@chemeng.iisc.ernet.in.

defined as $\psi=(c_w-c_o)/(c_w+c_o)$, where c_w and c_o are the concentrations of the hydrophilic and hydrophobic components. We assume that the system is incompressible, so that the total concentration c_w+c_o is a constant. In this case, the concentration field varies in the range $-1\leq\psi\leq+1$. The free energy functional is chosen so that a periodic modulation in ψ of wavelength equal to the layer spacing is obtained at equilibrium. For simplicity, we use a "symmetric" free energy functional in which the widths of the hydrophilic and hydrophobic parts are equal, although this restriction can be easily relaxed. The form of the ψ wave depends on the parameters chosen in the free energy functional; a sine wave is obtained at one extreme, while a square wave is obtained at the other extreme. In a molecular system, this corresponds to the transition between a diffuse lamellar phase with a lot of hydrophilic-hydrophobic interpenetration and to a frozen lamellar phase with no hydrophilic-hydrophobic interpenetration. Quantitative measures are devised to relate the concentration profiles obtained in molecular dynamics to the corresponding parameters in the free energy functional.

The free energy functional also contains an energy scale, which determines the departures in the free energy from the energy minimum due to concentration fluctuations. Fluctuations are defined by a displacement field, which measures, locally, the displacement of the layers from their equilibrium positions. Fluctuations in an ordered lamellar phase can be of two types, layer compression in the direction perpendicular to the plane of the layers and layer bending along the plane of the layers. The stress due to the layer compression is proportional to the product of the "compression modulus" and the second spatial derivative of the layer-displacement field along the layer normal direction. For a tensionless membrane, the stress due to bending is proportional to the "bending modulus" and the fourth spatial derivative of the layer-displacement field. The relationship between these moduli and the parameters in the free energy functional in the mesoscale description is derived. It is also shown how the energy scale can be obtained from the bending modulus calculated from molecular simulations, which is related to the height-height correlations.

The dynamics of the system is governed by dynamical equations for the concentration and velocity fields. The parameters determining the dynamical response are the Onsager coefficient for the concentration field and the viscosity in the fluid momentum equation. In the mesoscale description, there are two dynamical parameters, the Onsager coefficient for the concentration field and the kinematic viscosity in the fluid momentum equation. The kinematic viscosity can be determined quite easily using standard procedures such as the Lees–Edwards boundary conditions in Non-Equilibrium Molecular Dynamics (NEMD) simulations. In order to obtain the Onsager coefficient, it is necessary to consider the relative motion of the hydrophilic and hydrophobic species or the transport of water through the surfactant bilayers in response to a pressure gradient. Data from previous molecular dynamics simulations are used to show how the Onsager coefficient can be calculated from the permeation constant in a molecular simulation.

The dynamical linear response to small perturbations is determined by calculating the dispersion relation. The response is anisotropic, and the decay rate of perturbations along the plane of the layers is different from that in the layer normal direction. Perturbations along the plane of the layers can relax due to flow along the layers, without relative motion of the hydrophilic and hydrophobic species. However, perturbations perpendicular to the plane of the layers can relax only by relative motion of the hydrophilic and hydrophobic parts, and therefore the relaxation rate depends on the permeation constant. More interestingly, the relaxation of oblique waves has a propagating component in addition to a diffusive component, and the sound speed that emerges from the decay rate (called the "second sound" speed) is related to the compression modulus. The relationship between the decay rates and the thermodynamic and dynamical parameters in the mesoscale description is explicitly derived in the present analysis.

At the mesoscale, we use the lattice-Boltzmann (LB) simulation[8] in order to verify our theoretical predictions. Here, we use an adaptation of this technique[3–7] to determine the evolution of the structure and rheology of lamellar liquid crystalline phases in flows of practical interest. We verify, in the simulations, that the wave form of the concentration variation is in agreement with theoretical predictions. We also verify that the bending and compression moduli predicted by the theory are in agreement with the simulations, by placing a small perturbation on the concentration field in the simulations and calculating the force density generated due to the perturbation. The decay rate of the perturbations, and, in particular, the speed of the second sound, is also explicitly calculated in the simulations; it is verified that there is quantitative agreement between theory and simulations. The simulations are restricted to two dimensional flows due to computational limitations, but could easily be extended to three dimensional flows as well.

It should be noted that lamellar mesophases are also encountered in block copolymer melts for certain fractions of the two blocks.[9] Block copolymers typically consist of two blocks of different polymers which are covalently linked. In these systems, there are two competing thermodynamic effects which determine the phase boundaries, the enthalpic repulsion between the two blocks which promotes segregation, and entropy which tends to homogenize the concentration field. In addition, since the two blocks are covalently linked, it is not possible to have complete phase segregation. Depending on the ratios of the number of monomers in each of the blocks, one could have different mesophases such as the micellar, lamellar, and hexagonal. In these cases, the free energy functional also contains the entropic term (Edwards Hamiltonian) which incorporates chain stretching effects. The concentration field undergoes a transition from a sine wave profile (weak segregation limit)[10] to a step function (strong segregation limit)[11] as the strength of the enthalpic repulsion between the two blocks is increased. This transition can be captured by the free energy functional used here for the surfactant lamellar mesophase. However, the elastic effects due to chain stretching in block copolymers are not present in the present formulation, and so the present model can be used to describe block copolymers only in the limit where elastic effects due to chain stretching are negligible.

At the macroscopic scale, it is infeasible to incorporate the details of the concentration fluctuations between the hydrophilic and hydrophobic parts in a continuum description. In the present analysis, we suggest additional fields which could be included, which are the layer spacing and the layer normal fields. Equations for the layer spacing and the layer normal fields are proposed, and the procedure for incorporating the stresses in the fluid momentum equation is suggested. Along the direction normal to the layers, it is shown that the equation for the layer displacement reduces to an equation similar to the Darcy equation for porous media, while there is an additional force density due to layer bending and compression in the momentum equation. The constants in the macroscopic equations are related to those in the mesoscale simulations. This provides a complete formulation of the multiscale modeling methodologies for lamellar mesophases.

Another issue of importance is the fluctuation corrections to the bending and compression moduli due to the cubic and quartic terms in the free energy functional which have been neglected in Eq. (2). It has been shown by Grinstein and Pelcovits,[12] using renormalization group in three dimensions, that the compression modulus goes to zero, and the bending modulus diverges. However, the divergences are proportional to a small power of the log of the system size. The compression modulus decreases to zero as $\log(L)^{2/5}$, while the bending modulus diverges as $\log(L)^{-1/5}$, where L is the system size (characteristic length of the ordered lamellar phase). Therefore, the renormalizations of the compression and bending modulus are small even for systems of sizes probed in experiments.[12] The system sizes in simulations are even smaller, and so renormalization effects are likely to be very weak in simulations.

We consider the specific example of the bending modulus for a perfectly ordered lamellar phase of length of 1 cm. It should be noted that this system size is a gross overestimate; it is very difficult to obtain a perfectly defect-free aligned sample of a lyotropic lamellar liquid crystal of size of 1 cm, and real samples will always have defects and microdomains whose size is, at most, 100 μm. The bending modulus shows a larger renormalization $(\log(L))^{2/5}$ in comparison to the compression modulus $(\log(L))^{-1/5}$, and so we examine the change in the bending modulus due to fluctuation effects. The calculation of Grinstein and Pelcovits showed that the bare bending modulus is multiplied by a factor $(1-0.017\log(\Gamma L))^{2/5}$, where Γ is the ultraviolet cutoff in the theory and L is the length of the system parallel to the layers, and Γ is the "ultraviolet cutoff" in the wave vector corresponding to the smallest length scale in the system. If we assume the smallest length scale is 10 nm, corresponding to the layer spacing in a typical lyotropic liquid crystal, and the system size is 1 cm, the bending modulus is changed only by about 8%. As noted above, the microdomains in real lyotropic liquid crystals are much smaller than 1 cm, and so the renormalization of the bending modulus will be very small even for systems encountered in practice. However, these corrections could be significant in other types of smectic and nematic liquid crystalline phases, such as the elastomer tubule phases.[13]

A related issue whether the terms in the Landau expansion included in the present description are sufficient for modeling a lamellar phase and whether the corrections due to the higher order terms are small. There are aspects which need to be discussed here. The first is with regard to the fluctuation renormalization of the bending and compression moduli due to the higher order contributions to the free energy functional. The renormalization has been studied by Grinstein and Pelcovits,[12] as discussed above, and it is found that the corrections to the bending and compression moduli very small and are proportional to small powers of the logarithm of the system size. These will be difficult to observe even macroscopic system sizes used in experiments. It should be noted that Grinstein and Pelcovits[12] only included the contributions to the free energy due to the nonlinear terms in the rotationally invariant strain tensor, within the context of linear elasticity theory. There do not seem to be detailed calculations of the terms which would be obtained if a nonlinear elasticity theory was used. However, the corrections to the bending and compression moduli would still be a logarithmic function of the system size because the upper critical dimension is three for this system.

The second issue is whether the thermodynamics and dynamics of the local concentration fields are adequately captured by the Landau free energy functional used here. In lyotropic liquid crystalline systems, there are often sharp interfaces between the hydrophilic and hydrophobic parts. Due to this, it is not a good approximation to model the concentration modulation as a single sine wave. In our analysis, we have used a formulation where the fundamental modulation and its higher harmonics are incorporated in the model, so there is a parameter which provides a transition from a sine wave to a series of step functions of equal magnitude and opposite signs. The formulation admits two length scales, one of which is the wavelength of the fundamental mode and the second small length scale is the interface thickness over which there is a transition from the hydrophilic to the hydrophobic parts. The latter is similar to the interface thickness in the square gradient theories for two immiscible fluids. In addition, there is the limitation that the system is incompressible, so that the concentration is independent of position across the layers. The present model will be able to capture the local concentration variations if these two approximations (incompressibility and the presence of only two length scales) are valid.

One important aspect that has not been considered here is the role of defects in the rheology of lamellar liquid crystalline systems. Even though a perfect defect-free stack of layers is the final equilibrium state, real samples are rarely defect-free due to kinetic constraints. The rheological properties are often determined more by defects such as grain boundaries, disclination lines, and focal conic defects than by the rheological properties of the background aligned lamellar phase.[14–16] The inclusion of these defects requires a description of mechanisms that both generate as well as anneal defects, which is outside the scope of the present work.

In order to compare our analysis with numerical simulations, we use the LB technique.[3–7] The details of the simulation technique are briefly discussed in Appendix, since they are quite standard. In Sec. II A, we discuss the concentration profiles that are obtained by the minimization of the free energy functional used here and the Fourier decomposition of these concentration profiles. The profiles obtained by a direct minimization of the free energy functional are compared to the profiles obtained from a complete LB simulation that includes both the concentration and the fluid momentum fields. In Sec. II B, the free energy functional for a macroscale description (in terms of the layer-displacement field) is obtained from the free energy functional expressed in terms of the concentration field, and expressions for the bending and compression moduli in the macroscale description are obtained in terms of the parameters in the free energy functional for the concentration field. An issue of importance here is the invariance of the macroscale free energy under layer tilt. Since there is no energy penalty for tilting the layers, the macroscale free energy should not contain any "surface tension" terms. When the coarse graining is done in a naive fashion, we do obtain a surface tension term in the most general case. We show that this can be removed either by renormalizing the wave number in the expression for the free energy or equivalently adding a square gradient term in the original free energy functional whose coefficient is chosen so that the surface tension is zero. The value of the coefficient is explicitly calculated. In this manner, we are able to obtain a consistent expression for the mesoscale free energy functional (in terms of the concentration field) which, when coarse grained, provides a macroscale free energy functional with no surface tension.

The coarse-graining procedure for the dynamical parameters is discussed in Sec. II C. Here, we write down the equivalent of the model-H (Ref. 17) equations for the concentration field and fluid momentum field in the mesoscale description. From this mesoscale description, a coarse-graining procedure is used to obtain dynamical equations for the layer-displacement field. The dynamical equations in the direction normal to the layers contain a permeation constant for the permeation of one phase through the second phase. This permeation constant is related to the Onsager coefficient in the mesoscale dynamical equation for the concentration field. In Sec. II D, we test whether the linear-response dispersion relations for the macroscale description (in terms of the layer-displacement field) can be correctly captured by a LB simulation which simulates the mesoscale concentration field. In this section, we impose perturbations on the concentration fields in directions parallel and perpendicular to the layer normal, as well as at intermediate angles. The relaxation rates of these perturbations are compared to the predictions of the macroscale dynamical equations for the layer-displacement fields. The LB simulation is able to correctly capture the decay of perturbations both parallel to and perpendicular to the layer normal direction. In addition, for perturbations with wave vector at an intermediate angle, we are also able to capture the propagating nature of the perturbations, which is referred to as second sound.

A proposed procedure for obtaining all the thermodynamic parameters in the free energy functional for the concentration field, as well as the dynamical parameters in the concentration and momentum equations, is discussed in Sec. III. In addition, the formulation of macroscale rheological equations, which are the equations for the evolution of the layer normal, layer spacing, and the fluid velocity field, is also discussed. These provide a way for progressing from molecular simulations for a single bilayer to the macroscale equivalent of the Navier–Stokes equations for a lamellar liquid crystalline fluid.

II. ANALYSIS

The free energy functional for the concentration field in the mesoscale description, required to produce a lamellar phase as the equilibrium solution, is

$$F[\psi]=A\int dV\left(-\frac{\psi^2}{2}+\frac{\psi^4}{4}+\frac{g}{2k^2}(\nabla\psi)^2+\frac{r}{2k^4}((\nabla^2+k^2)\psi)^2\right). \tag{1}$$

Here, we have defined the concentration field ψ and the parameters g and r to be dimensionless, while k has dimensions of the inverse of length. The parameter A represents an energy density (energy per unit volume), and this parameter sets the energy scale in the system. The first two terms on the right side of the above equation are the usual quadratic and quartic terms in a Landau–Ginzburg free energy, which results in segregation in a binary fluid due to the negative sign in the first term on the right side of Eq. (1). The third term on the right side is the surface tension terms, while the last term promotes the formation of interfaces with wavelength $(2\pi/k)$. It should be noted that the form in Eq. (1) is general; any general free energy functional of the form

$$F[\phi]=\int dV\left(-\frac{a'\phi^2}{2}+\frac{b'\phi^4}{4}+\frac{g'}{2}(\nabla\psi)^2+\frac{r'}{2}((\nabla^2+k^2)\psi)^2\right) \tag{2}$$

can be reduced to the form Eq. (1) by just rescaling the variables, i.e., by defining $\psi=(b/a)^{1/2}\phi$, $A=(a^2/b)$, $g=(g'k^2/a')$, and $r=(r'k^4/a')$.

Another important point to note is that the free energy functional in Eq. (1) is equivalent, to within an additive constant, to the form

$$F[\psi]=A\int dV\left(-\frac{a'\psi^2}{2}+\frac{\psi^4}{4}+\frac{r}{2k^4}((\nabla^2+k'^2)\psi)^2\right), \tag{3}$$

where k' is a renormalized layer spacing, which is given by

$$k'=\sqrt{k^2-\frac{g}{2r}} \tag{4}$$

and

$$a'=1+\frac{g}{2}-\frac{g^2}{4r}. \tag{5}$$

Therefore, the effect of the term proportional to g in Eq. (1) is just to renormalize the wave number of the modulation in the lamellar phase, in addition to altering the coefficient a'

multiplying the quadratic term in the free energy functional. However, we can change the coefficient of the quadratic term from a' to 1 by rescaling the concentration amplitude, as shown in going from Eq. (2) to Eq. (1). Therefore, a free energy functional with a nonzero value of g in Eq. (1) can be reduced to a functional with a zero value of g by renormalizing the wave number of the perturbations. This distinction is important because the form in Eq. (3) (or 1 with $g=0$) is rotational frame invariant, which implies that there should be no penalty for the tilt of all the layers by a constant angle. This is a requirement we also impose on the layer-displacement field a little later and show how the value of g in Eq. (1) (or, alternatively, the modified wave number in Eq. (3)) has to be chosen to render the free energy invariant when the layers are tilted.

At the macroscopic scale, the dynamical variable used is the unit normal to the layers $\mathbf{n}$, which is perpendicular to the plane of the layers at every point, and the layer-displacement field u, which is the displacement of the layers from their equilibrium positions. The reference plane for the layer-displacement field is arbitrary, since a constant translation of all the layers does not change the total free energy. Therefore, the free energy changes and the stresses generated depend only on the variation of u in the directions tangential and normal to the layers. In order to write down the free energy for small displacements, we choose a coordinate system in which the coordinates x and y are locally tangential to the layers and z is perpendicular to the plane or the layers. We also use the notation $u_x=(\partial u/\partial x)$, $u_y=(\partial u/\partial y)$, and $u_z=(\partial u/\partial z)$; a larger number of subscripts represents repeated derivatives with respect to the position variables. The free energy functional for this correct to second order in u can be written, using symmetry arguments, as

$$F[u]=F_0+\int dV\left(\frac{Bu_z^2}{2}+\frac{G(u_x^2+u_y^2)}{2}+\frac{K(u_{xx}+u_{yy}+u_{zz})^2}{2}\right). \tag{6}$$

Here, the first term in the integral on the right side of Eq. (6) imposes a penalty for displacements normal to the layers which tend to compress or expand the layers and B is the layer compression modulus. The second term in the integral on the right side of Eq. (6) represents the free energy change due to a change in area along the layers, and G is the surface tension. The third term in the integral on the right is the change in energy due to bending of the interface and K is the curvature modulus. While analyzing single membrane fluctuations, the free energy functional is sometimes written as an integral over the area of the membrane,

$$F[u]=F_0+\int dA\left(\frac{B_Au_z^2}{2}+\frac{G_A(u_x^2+u_y^2)}{2}+\frac{K_A(u_{xx}+u_{yy}+u_{zz})^2}{2}\right). \tag{7}$$

It is easy to verify the relations $B=(B_A/\lambda)$, $G=(G_A/\lambda)$, and $K=(K_A/\lambda)$, where λ is the layer spacing. The objective of the analysis is to determine the relations between B, G, and K from a knowledge of the parameters in the microscopic free energy functional in Eq. (1) which is written in terms of the concentration field.

In a real lyotropic liquid crystalline fluid, the surface tension is zero, in order to ensure that the free energy is invariant when the layers are tilted (displacement u is proportional to the coordinate x along the layers, so that u_x is a constant). This implies that the coefficient G in Eq. (7) has to be zero. Our analysis shows that when we do coarse graining of a free energy functional of the type Eq. (6), with $g=0$, we obtain a nonzero value of G in Eq. (6) in the most general case. One of the objectives of the present analysis was to determine what are the parameters in the mesoscopic free energy functional, Eq. (1), to be used so that the surface tension is zero in the coarse-grained expression, Eq. (7). Naively, it might be expected that if the parameter g in Eq. (2) is equal to zero, then the surface tension term in Eq. (7) will also be equal to zero. Our analysis shows that this is true only in the limit where the parameter r in Eq. (1) becomes very large, so that the concentration amplitude is very well approximated by a single sine function with wavelength equal to the total layer spacing. When r in Eq. (1) becomes small, so that the concentration field is well approximated by a series of step functions, then it is necessary to have a nonzero and negative value of g (equal to g_0 shown in Fig. 3 a little later) in order to obtain the zero tension state. Note that the nonzero value of g in Eq. (1) also introduces a modification of the wave vector $k'=\sqrt{k^2-(g/2r)}$ in Eq. (3). Since g is negative, the layer spacing $(2\pi/k')$ is smaller than the original layer spacing $(2\pi/k)$ used in Eq. (1). It is possible to work with a free energy functional of the type (3) (with $g=0$) instead of an equation of the type (1), but the wave number in Eq. (3) is different from that in the coarse-grained description (6). Therefore, we prefer to use the free energy functional 1, with the value of g chosen so that $G=0$ in Eq. (6). This provides us with a consistent procedure for obtaining the zero tension state even when the interface between the hydrophobic and hydrophilic phases is sharp, and the concentration field is very different from a sine wave.

A. Concentration profiles

First we examine the concentration profile for the equilibrium state for the free energy functional (1), which can be determined by minimizing $F[\psi]$ with respect to variations in ψ,

$$\frac{\delta F}{\delta\psi}=0. \tag{8}$$

Using the Euler–Lagrange equations, we obtain the following cubic form for the concentration field ψ:

$$-\psi+\psi^3-g\nabla^2\psi+r(\nabla^4+2k^2\nabla^2+k^4)\psi=0. \tag{9}$$

First, we note that the last term on the left side of Eq. (9) is zero for a sinusoidal variation with wave number k, and therefore if r is large, we would expect the equilibrium profile to be a sinusoidal modulation with wave number k. However, there will be a generation of higher harmonics due to the first two terms on the left side of Eq. (9), and the most

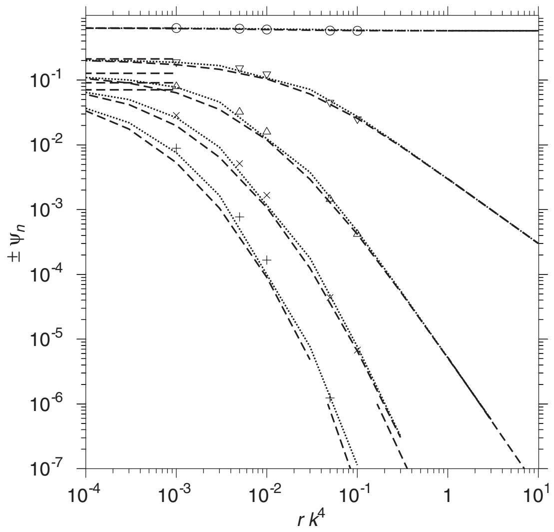

FIG. 1. The coefficients $\pm\psi_n$ as a function of the parameter r. ○: ψ_1; ■: $-\psi_3$; ∇: ψ_5; ▷: $-\psi_7$; ◁: ψ_9; ◇: $-\psi_{11}$; ×: ψ_{13}; +: $-\psi_{15}$.

general concentration profile will be of the form

$$\psi=\sum_{n=0}^{\infty}\psi_n\exp(\imath nkz). \tag{10}$$

This is inserted into Eq. (9), and the coefficients of the terms with equal powers of $\exp(\imath nkz)$ are set equal to zero in order to obtain solutions for ψ_n which are a function of r. From symmetry considerations, it can be inferred that $\psi_{-n}=\psi_n$, since the concentration field has to be real, and $\psi_0=0$ since the total concentration is zero for a symmetric binary mixture.

The coefficients ψ_n and the concentration profiles were evaluated numerically for "zero surface tension" case for which g and r are related as shown in Eq. (17) a little later. The formulation of the zero tension case is discussed a little later; at this point, it is sufficient to note that the dynamics of the bilayers described by the free energy functional 1 has a positive surface tension for $g=0$, and it is necessary to set g equal to a negative value for the zero tension state. The coefficients ψ_n were numerically evaluated as follows. The series in Eq. (9) was truncated at $n=15$, and eight simultaneous nonlinear equations were obtained. These were solved iteratively using a Newton–Raphson procedure in order to obtain the coefficients ψ_n from $n=1$ to $n=15$. In the iterative procedure, the initial guesses for the coefficients were chosen as follows. In the limit $r \gg 1$, the first and second terms on the left of Eq. (9) can be neglected in comparison to the fourth term, and the solution for the concentration field is a cosine wave with wave number k. In this case, the coefficient $\psi_1 =(1/\sqrt{3})$, and all other coefficients are equal to zero. The solution for $r=10$ was first obtained using the starting guess $\psi_1=(1/\sqrt{3})$, $\psi_n=0$ for $n\neq 1$. Then, the parameter r was progressively reduced by factors of 2 using the solution for a given value of r as the starting guess for $(r/2)$, in order to obtain the coefficients ψ_n. These coefficients are shown as a function of r in Fig. 1. The concentration profiles obtained for different values of r are shown in Fig. 2. As anticipated, the concentration profile is close to a sinusoidal profile for $r\geq 1$, but becomes close to a step profile as r decreases.

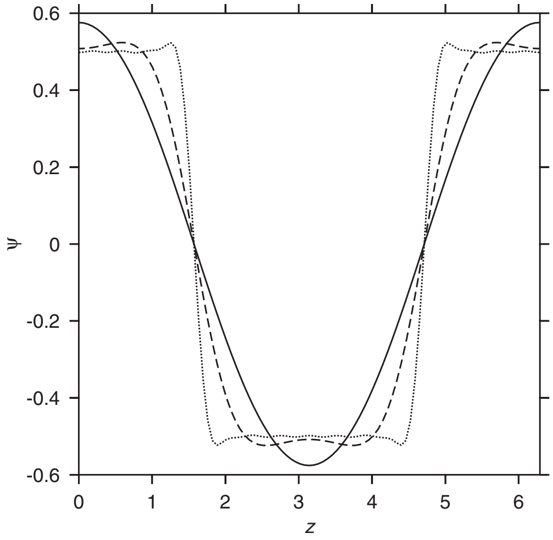

FIG. 2. The concentration ψ as a function of distance z for different values of the parameter r. Solid line: $r=1$; dashed line: $r=10^{-2}$; dotted line: $r=10^{-4}$.

It is instructive to first examine the asymptotic behavior of the solutions in the limits $r \gg 1$ and $r \ll 1$. For a square wave in the limit $r \ll 1$, the coefficients ψ_n can be calculated quite easily,

$$\begin{aligned}\psi_n &= \frac{(-2)^{(n-1)/2}}{\pi n}\quad \text{for odd } n,\\ &=0 \quad \text{for even } n.\end{aligned} \tag{11}$$

The above results are shown by the dashed lines on the left side of Fig. 1. It is observed that the numerical results for $n=1$, $n=3$, and $n=5$ converge to the asymptotic results for $r=10^{-4}$, but the higher harmonics have still not converged to the asymptotic values. In the limit $r \gg 1$, we can use an asymptotic expansion in r^{-1} in order to obtain the following solutions for ψ_n for $1\leq n\leq 9$:

$$\begin{aligned}\psi_1 &= \frac{1}{\sqrt{3}},\\ \psi_3 &= \frac{-1}{192\sqrt{3}r},\\ \psi_5 &= \frac{1}{110\,592\sqrt{3}r^2},\\ \psi_7 &= \frac{-1}{127\,401\,984\sqrt{3}r^3},\\ \psi_9 &= \frac{7}{815\,372\,697\,600\sqrt{3}r^4}.\end{aligned} \tag{12}$$

These above results are shown by the dashed lines on the right side of Fig. 1. It is observed that there is an excellent agreement between the asymptotic and numerical results even when ψ_n is as low as 10^{-7}. The results of the Lattice-

Boltzmann method (LBM) simulations for the concentration profiles are found to be in excellent agreement with the numerical profiles over the entire range of the parameter r.

B. Bending and compression moduli

In order to extract the layer compression and bending moduli from this free energy functional, we propose a small perturbation about this equilibrium solution of the form

$$\psi = \sum_{n=-\infty}^{\infty} \psi_n \exp(\imath nk(z - u(x,y,z,t))), \tag{13}$$

where u is the layer-displacement field in the z direction. This is inserted into the expression for the free energy and simplified as follows. The derivatives of the concentration fields in the z and x directions, using chain rule, are

$$\partial_z \psi = \sum_{n=-\infty}^{\infty} (\imath nk(1-u_z)\psi_n \exp(\imath nk(z-u))),$$

$$\partial_z^2 \psi = \sum_{n=-\infty}^{\infty} (-n^2k^2(1-u_z)^2 - \imath nku_{zz})\psi_n \exp(\imath nk(z-u)),$$

$$\partial_x^2 \psi = \sum_{n=-\infty}^{\infty} (-n^2k^2u_x^2 - \imath nku_{xx})\psi_n \exp(\imath nk(z-u)). \tag{14}$$

Using these, $(\nabla^2+k^2)\psi$ can be written as

$$(\nabla^2+k^2)\psi = \sum_{n=-\infty}^{\infty} ((1-n^2)k^2 + 2n^2k^2(u_z - (1/2)(\nabla u)^2) - \imath nk\nabla^2 u)\psi_n \exp(\imath nk(z-u)), \tag{15}$$

where $(u_z-(1/2)(\nabla u)^2)$ is the zz component of the frame-invariant strain tensor. In the following analysis, we will retain only terms correct to linear order in the above expansion.

We insert the above expansions into the free energy functional 1, expand in a series in small u, and include terms that are quadratic in u and its derivatives. Further, we assume that the length scale for the variation in the u field is large compared to the layer spacing $\lambda=(2\pi/k)$. If we integrate over lengths comparable to the λ to obtain a coarse-grained free energy functional, all terms in the free energy functional proportional to $\exp(\imath mkz)$ for $m\neq 0$ will average to zero. Then, we will be left only with terms which do not have any modulation over distances comparable to λ, and we recover a free energy functional of the form 6, in which the constants B, K, and G are given by

$$B = A\sum_{n=-\infty}^{\infty} (2rn^2(3n^2-1) + gn^2)\psi_n^2,$$

$$K = A\sum_{n=-\infty}^{\infty} (rn^2/k^2)\psi_n^2, \tag{16}$$

$$G = A\sum_{n=-\infty}^{\infty} (2rn^2(n^2-1) + gn^2)\psi_n^2.$$

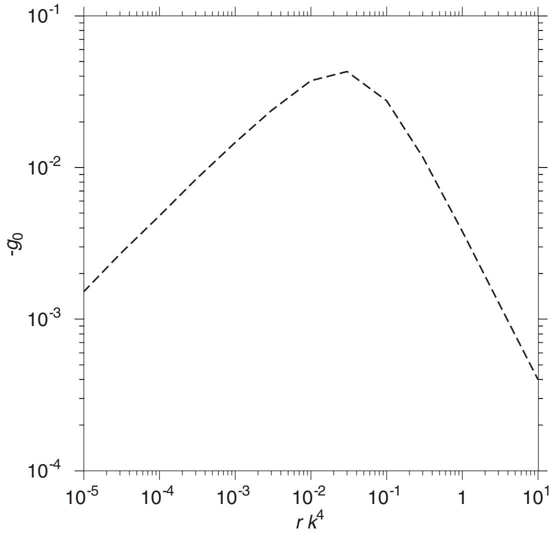

FIG. 3. The variation in $-g_0$ with r, where g_0 is the value of g in the free energy functional (1) which corresponds to a zero tension state.

Clearly, the surface tension in the macroscopic description has contributions from both the term proportional to r and the term proportional to g in the free energy functional (1), whereas the bending modulus depends only on r. In order to achieve a tensionless state, it is necessary to construct the free energy functional with the parameter g chosen so that

$$g = g_0 = -\frac{\sum_{n=-\infty}^{\infty} 2rn^2(n^2-1)\psi_n^2}{\sum_{n=-\infty}^{\infty} n^2\psi_n^2}. \tag{17}$$

For this choice of parameters, the bending modulus would be

$$B = A\sum_{n=-\infty}^{\infty} 4rn^4\psi_n^2. \tag{18}$$

The value of g_0 is shown as a function of r in Fig. 3. The physical reasons for the scaling behavior of g_0 as a function of r in the limits $r \gg 1$ and $r \ll 1$ is as follows. In the limit $r \gg 1$, the contribution to g_0 in Eq. (17) proportional to ψ_1^2 is equal to zero, and so the largest nonzero contribution is the one proportional to ψ_2^2. From Eq. (12), it is clear that $\psi_2^2 \propto r^{-2}$, and therefore, we find that $g_0 \propto r^{-1}$ in the limit $r \gg 1$. In the limit $r \ll 1$, the concentration profile approaches a step function, as shown in Eq. (11). For a perfect step function $(r=0)$, the coefficients ψ_n decrease proportional to $(1/n)$. However, when r is small but nonzero, Eq. (11) is valid only for $n \ll r^{-1/4}$. This is because Eq. (11) was obtained assuming that the term proportional to r in Eq. (9) can be neglected. For a small but nonzero value of r, the term proportional to r on the left side of Eq. (9) becomes comparable to the other terms for $n \sim r^{-1/4}$. This can be adequately represented by a cutoff at $n \sim r^{-1/4}$ of the series expansion (17), when ψ_n is given by Eq. (11). When this upper limit for n is inserted into Eq. (17), it can easily be deduced that $g_0 \propto r^{1/2}$ in the limit $r \ll 1$. This scaling behavior is reproduced by the numerical calculations in Fig. 3.

In the limit $r \gg 1$, Eq. (12) indicates that $\psi_n \sim r^{(-(n-1)/2)}$. From Eq. (16), the bending and compression moduli are both proportional to Ar in this limit,

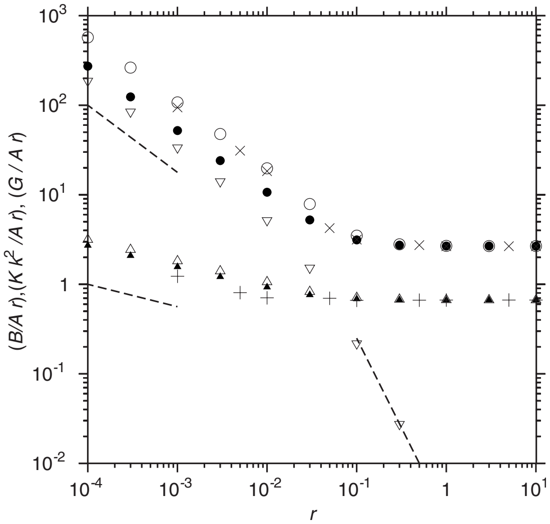

FIG. 4. The scaled compression modulus $(B/(Ar))$ (○) the scaled bending modulus $(Kk^2/(Ar))$ (△) as a function of r for the zero tension case $g=-g_0$ (filled symbols). The upper and lower dashed lines on the left show slopes of -0.75 and -0.25, respectively, and the dashed line on the right shows a slope of -2. The crosses show the results for the bending modulus, and the pluses show the compression modulus, obtained from LBM simulations on a system with 416×416 nodes and 13 lamellae, with $\tau=1$, $\tau_g=1$, and $\Gamma=1$. The compression and bending moduli and the nonzero surface tension are also shown for the case $g=0$ by the open symbols, where the scaled surface tension (G/Ar) is shown by the symbol ∇.

$$B \sim (Ar),$$
$$K \sim (Ar/k^2). \tag{19}$$

In the limit $r \ll 1$, Eq. (11) indicate that $\psi_n \propto n^{-1}$. However, this scaling is cutoff due to the gradient terms in the expression (9) for the concentration field. For $g \sim r^{1/2}$, it was shown in the previous paragraph that the upper limit for n_c which scales as $n_c \sim r^{-1/4}$ and the bending and compression moduli can be calculated using this upper cutoff for n are

$$B = A\sum_n 4rn^4\psi_n^2 \sim Arn_c^3 \sim Ar^{1/4}, \tag{20}$$

$$K = A\sum_n (r/k^2)n^2\psi_n^2 \sim A(r/k^2)n_c \sim A(r^{3/4}/k^2). \tag{21}$$

The bending and compression moduli scaled by (Ar) are shown as a function of the r in Fig. 4 for the case $g=g_0$. It is observed that both (B/Ar) and $(Kk^2/(Ar))$ approach constant values in the limit $r \gg 1$, as anticipated in Eq. (19). In the limit $r \ll 1$, we find that (B/Ar) and (G/Ar) increase proportional to $r^{-3/4}$, while (Kk^2/Ar) increases proportional to $r^{-1/4}$, as obtained in Eqs. (20) and (21). For completeness, we also show the scaling behavior of the moduli for the case where $g=0$. It is clearly observed that the surface tension G is not equal to zero in this case and could be quite large for $r \ll 1$, if the wave number is not correctly renormalized while going from the mesoscale to the macroscale description.

C. Dynamics

In order to consistently model the evolution of the concentration and momentum fields, we use equations similar to the model-H equations for a binary fluid, but with the free energy functional (1) which favors the formation of a lamellar phase. The dynamical equation for the concentration field ψ can be written as

$$\frac{\partial\psi}{\partial t} + \mathbf{v}\cdot\nabla\psi = -\nabla\cdot\mathbf{J}_\psi, \tag{22}$$

where the flux $\mathbf{J}_\psi$ for the concentration field is of the form

$$\mathbf{J}_\psi = -\Gamma\nabla\mu. \tag{23}$$

where Γ is the Onsager coefficient and the chemical potential $\mu=(\delta F/\delta\psi)$. Substituting the equation for the flux (23) into the concentration equation, we obtain

$$\frac{\partial\psi}{\partial t} + \mathbf{v}\cdot\nabla\psi = \Gamma\nabla^2\left(\frac{\delta F}{\delta\psi}\right). \tag{24}$$

The fluid equations are the modified Navier–Stokes mass and momentum equations, in which the momentum equation contains an additional term due to the concentration field. The mass conservation equations just ensure that the velocity field $\mathbf{v}$ is divergence free,

$$\nabla\cdot\mathbf{v} = 0, \tag{25}$$

while the momentum conservation equation is of the form

$$\rho\left(\frac{\partial\mathbf{v}}{\partial t} + \mathbf{v}\cdot\nabla\mathbf{v}\right) = -\nabla p + \mu\nabla^2\mathbf{v} + \nabla\psi\frac{\delta F}{\delta\psi}. \tag{26}$$

In the above equation, ρ and μ are the density and viscosity, p is the fluid pressure, and the last term on the right side of the above equation represents a force density due to the concentration field, which is required to ensure that Eqs. (24) and (26) satisfy the Poisson bracket relations.

At the macroscopic level, we write down equations for the fluid velocity field and the layer-displacement field u. In accordance with the analysis so far, we consider perturbations of the layers about their equilibrium state in which they are aligned in the x-y plane, and the layer normal is in the z direction. A displacement in the layers causes a restoring force density (force per unit volume) in the z direction, f_z, which is of the form

$$f_z = -\frac{\delta F}{\delta u} = Bu_{zz} - K\nabla^4 u. \tag{27}$$

This would result in a motion of the layers relative to the fluid; however, this motion has to take place due to the permeation of the fluid through the layers. Therefore, one would expect the flow of the fluid through the layers to be describe by a Darcy law of the form

$$\left(\frac{\partial u}{\partial t} - v_z\right) = Pf_z. \tag{28}$$

The additional force density f_z also exerts a force on the fluid, which should result in an additional term in the fluid momentum equation of the form

$$\rho\left(\frac{\partial \mathbf{v}}{\partial t}+\mathbf{v}\cdot\nabla\mathbf{v}\right)=-\nabla p+\mu\nabla^2\mathbf{v}+f_z. \tag{29}$$

In the present section, we verify that Eqs. (28) and (29) can be obtained from the concentration and momentum equations (24) and (26) and derive a relation between the permeability P in Eq. (28) and the Onsager coefficient Γ in Eq. (24).

Using the form Eq. (13) for the concentration fields, and retaining only terms that are linear in u and $\mathbf{v}$, we obtain

$$\begin{aligned}\sum_{n=-\infty}^{\infty}(-\imath nk\psi_n\exp(\imath nkz))\left(\frac{\partial u}{\partial t}-v_z\right)&\\ =\Gamma A\sum_{n=-\infty}^{\infty}&(-n^2k^2\psi_n\exp(\imath nkz))((-\imath nr/k^3)(\nabla^4u)\\ &+(2(\imath nr/k)(3n^2-1)+(\imath ng/k))u_{zz}\\ &+(2(\imath nr/k)(n^2-1)+(\imath ng/k))u_{xx}).\end{aligned} \tag{30}$$

Since all the Fourier modes are orthogonal to each other, we obtain, for each value of n,

$$\begin{aligned}\psi_n\exp(\imath nkz)\left(\frac{\partial u}{\partial t}-v_z\right)&\\ =-\Gamma A\psi_n&\exp(\imath nkz)((rn^2/k^2)(\nabla^4u)\\ &-(2rn^2(3n^2-1)+n^2g)u_{zz})\\ &-((2rn^2(n^2-1)+n^2g)u_{xx}).\end{aligned} \tag{31}$$

In order to obtain the equations for the long wave limit, we multiply each equation in the above series by $\psi_{-n}\exp(-\imath nkz)$ and sum over all n to obtain

$$\left(\sum_{n=-\infty}^{\infty}\psi_n^2\right)\left(\frac{\partial u}{\partial t}-v_z\right)=-\Gamma(-Bu_{zz}+K\nabla^4u). \tag{32}$$

Clearly, Eq. (32) has the same form as Eq. (28), and the above calculation shows that the macroscopic equation (28) can be obtained from the concentration equation (24) with the permeation constant

$$P=\frac{\Gamma}{(\Sigma_{n=-\infty}^{\infty}\psi_n^2)}. \tag{33}$$

An interesting point to note that the permeation constant in Eq. (28) has the same dimensions as the Onsager coefficient in Eq. (24). The ratio (P/Γ) is shown as a function of r for in Fig. 5. This ratio tends to a constant value of 1.5 in the limit $r\gg 1$, where the amplitudes ψ_n are given by Eq. (12). In the limit $r\gg 1$ (11), it is easy to verify that (P/Γ) tends to a constant value of 1. Therefore, the ratio of the permeability and the Onsager coefficient does not show much variation as the value of r is varied. These scalings are consistent with the numerical results shown in Fig. 5.

Next, we turn to the fluid momentum equation. If the equation for the concentration field (13) is substituted into the fluid momentum equation (26), and only terms linear in the displacement field u are retained, we obtain

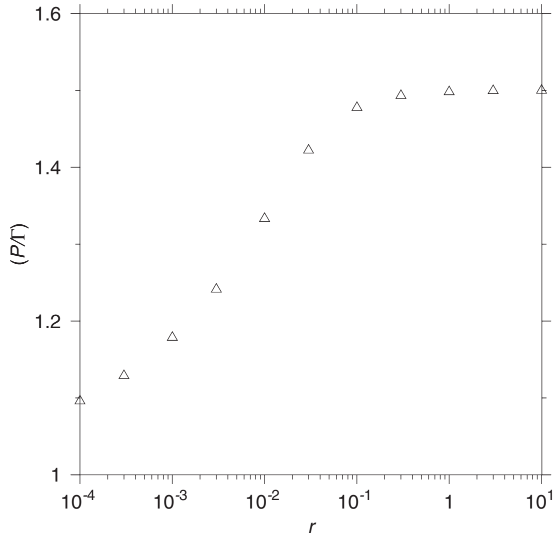

FIG. 5. The ratio (P/Γ) as a function of r the zero tension case $g=g_0$ (△).

$$\begin{aligned}\rho\left(\frac{\partial \mathbf{v}}{\partial t}+\mathbf{v}\,.\,\nabla\mathbf{v}\right)&\\ =-\nabla p+\mu\nabla^2\mathbf{v}+&\sum_{m=-\infty}^{\infty}\sum_{n=-\infty}^{\infty}(\imath mk\psi_m\exp(\imath mkz))\\ &\times(((2(\imath rn/k)(3n^2-1)+(\imath gn/k))u_{zz}\\ &+((2\imath rn/k)(n^2-1)+(\imath gn/k))(u_{xx}+u_{yy})\\ &-(\imath rn/k^3)\nabla^4u)\exp(\imath nkz)\psi_n).\end{aligned} \tag{34}$$

In order to obtain the macroscopic momentum conservation equation, we take the zero wavelength limit of the above equation, which is equivalent to setting $m=-n$ on the last term on the right side. With this operation, we obtain the macroscopic momentum equation as

$$\rho\left(\frac{\partial \mathbf{v}}{\partial t}+\mathbf{v}\cdot\nabla\mathbf{v}\right)=-\nabla p+\mu\nabla^2\mathbf{v}+(Bu_{zz}-K\nabla^4u), \tag{35}$$

where B and K are given by Eq. (16). Thus, we obtain the macroscopic momentum equation (29) from the microscopic equation (26).

D. Linear response

In this section, we analyze the linear response of the macroscopic equations for the lamellar displacement and fluid velocity fields and determine the dispersion relations. For this purpose, we assume two dimensional perturbations to the lamellar displacement and fluid velocity fields of the form

$$\begin{aligned}u&=\tilde{u}\exp(st)\exp(\imath(q_xx+q_zz)),\\ \mathbf{v}&=\tilde{\mathbf{v}}\exp(st)\exp(\imath(q_xx+q_zz)).\end{aligned} \tag{36}$$

Here, it is assumed that q_x and q_z are small compared to k, so that the wavelengths of the perturbations are long compared to the lamellar spacing. When these forms of the perturbation equations are inserted into the equation for the layer displacement (28), and linearized, we obtain

$$(s\tilde{u} - \tilde{v}_z) = -(Bq_z^2 + Kq^4)\tilde{u}, \tag{37}$$

while the linearized fluid mass and momentum equations, (25) and (26), are

$$q_x\tilde{v}_x + q_z\tilde{v}_z = 0, \tag{38}$$

$$\rho s\tilde{v}_z = -\imath q_z\tilde{p} - \mu q^2\tilde{v}_z - (Bq_z^2 + Kq^4)\tilde{u}, \tag{39}$$

$$\rho s\tilde{v}_x = -\imath q_x\tilde{p} - \mu q^2 v_x, \tag{40}$$

where $q=\sqrt{q_x^2+q_z^2}$. The pressure can be eliminated from the momentum equations by taking $q_x \times 39 - q_z \times 40$ and using Eq. (38) to express $\tilde{v}_x$ in terms of $\tilde{v}_z$. This can be combined with Eq. (37) for the layer-displacement field to obtain the dispersion relation

$$\rho q^2(s + \nu q^2)(s + P(Bq_z^2 + Kq^4)) + q_x^2(Bq_z^2 + Kq^4)\tilde{u} = 0, \tag{41}$$

where ν, the kinematic viscosity, is (μ/ρ).

It is useful to first analyze the growth rate for perturbations along and perpendicular to the layers. For perturbations perpendicular to the layers, we set $q_x=0$ and obtain two solutions for the growth rate, which to lowest order in the small q expansion are

$$s_1 = -\nu q^2,$$
$$s_2 = -PBq_z^2. \tag{42}$$

It is clear that perturbations perpendicular to the plane of the layers decay diffusively, since the decay rates are proportional to the square of the wave number. The first solution s_1 corresponds to viscous relaxation, while the second solution s_2 represents the relaxation of the displacement field in response to an expansion or compression in the direction normal to the layers. For perturbations along the layers $(q_z=0)$, we find that the solutions for s are of the form

$$s = -\frac{q_x^2(\nu \pm \sqrt{\nu^2 - 4(K/\rho)})}{2}. \tag{43}$$

These modes are also diffusive, since the relaxation rates of these modes are also proportional to q_x^2. For oblique modes with nonzero (q_x, q_z), we find that the perturbations are propagating for the zero tension case,

$$s = \pm \imath (q_x q_z/q)\sqrt{B/\rho} - \frac{(PBq_z^2 + \nu q^2)}{2}. \tag{44}$$

Equation (44) shows that the decay of perturbations depends on the ratio (q_z/q_x) or on the angle of the perturbation wave with respect to the layer normal, which is given by $\theta = \arctan(q_x/q_z)$. The decay is exponential for perturbations of both the compression and bending types, $\theta=0$ and $(\pi/2)$, shown in Fig. 6(a) and 6(b). However, for $0 < \theta < (\pi/2)$, the imaginary part of s in Eq. (44) is nonzero, and perturbation relaxation has an oscillatory behavior.

Figure 4 shows the results of LBM simulations for the bending and compression moduli obtained using Eq. (27). The simulations were carried out in a two dimensional simulation box with 416×416 nodes, with a total of 13 lamellae. The simulation parameters used were $\tau=1$, $\tau_g=1$, and $\Gamma=1$, and the parameter r in the free energy functional was varied. A perturbation of the type shown in Eq. (13) was placed on the equilibrium state. The displacement field u was chosen to be of the form (36), with the amplitude $\tilde{u}$ set equal to 0.1 times the lamellar thickness; it was verified that the we are in the linear relaxation regime for this value of $\tilde{u}$. The force density caused due to this perturbation was determined, and the bending and compression moduli were determined from Eq. (27). The wavelength of the perturbation was assumed to be $q_x=(k/13), q_z=0$ and $q_x=0, q_z=(k/13)$, respectively, for the bending and compression modes, where k is the wave number for the lamellar modulation in the base state. As indicated in Fig. 4, there is quantitative agreement between the theoretical predictions and the simulation results for the bending and compression moduli.

The relaxation of perturbations that are neither along nor perpendicular to the layers is shown in Fig. 7, where the time is in lattice units. The simulations were carried out in a two dimensional simulation cell with 128 nodes in the z (layer normal) direction and with the notes in the x direction suitably chosen between 128 and 478 nodes in order to fit one perturbation wave in the x direction into the cell. The bilayer spacing was set equal to eight nodes, so that 16 bilayers fit into one simulation cell. The value of $r=10$ was used for the simulations, and the relaxation times used were $\tau_1=0.51$ and $\tau_2=1.0$. Figure 7 shows the value of (ψ/ψ_0) at the center of the simulation cell, where the perturbation applied is a maximum. It is clearly observed that the perturbation has an oscillatory nature for oblique waves, and the frequency of perturbations increases from $\theta=(\pi/3)$ to $\theta=(\pi/4)$, and then decreases again as θ is increased to $(\pi/6)$.

The "wave speed" c_s is defined as the ratio of the imaginary part of the growth rate (44) and the magnitude of the wave number q. From Eq. (44), we obtain

$$c_s = (q_x q_y/q)\sqrt{B/\rho} = \sqrt{B/\rho}\cos(\theta)\sin(\theta). \tag{45}$$

The wave speed of this mode is referred to as 'second sound' speed, in analogy with the speed of sound for longitudinal perturbations in a simple fluid. The sound speed is shown as a function of the angle θ in Fig. 8. This is a polar plot, where the polar coordinate represents the angle from the vertical, and the radial coordinate is the ratio $(c_s/\sqrt{B/\rho})$. It is clearly observed that the sound speed is zero for both $\theta=0$ and $\theta=(\pi/2)$, while it has a maximum at $\theta=(\pi/4)$. Also shown in the figure are the simulation results from the LB simulations for two different values of r in the free energy functional (1); the circles show the results for $r=100$ and the crosses show the results for $r=0.001$. There is a good quantitative agreement between simulations and theory with no fitted parameters; there is an error of about 6%–7% between the theoretical and experimental results. This error is expected from the finite differencing scheme we are using for calculating the derivatives; the width of the bilayer was eight LB nodes in the simulations, and so one would expect an error in the calculation of derivatives of about 6%–7%. The error is larger for $r=0.001$, primarily because the numerical errors in the finite difference scheme are larger due to the sharper gradients in the concentration equation. However, the quali-

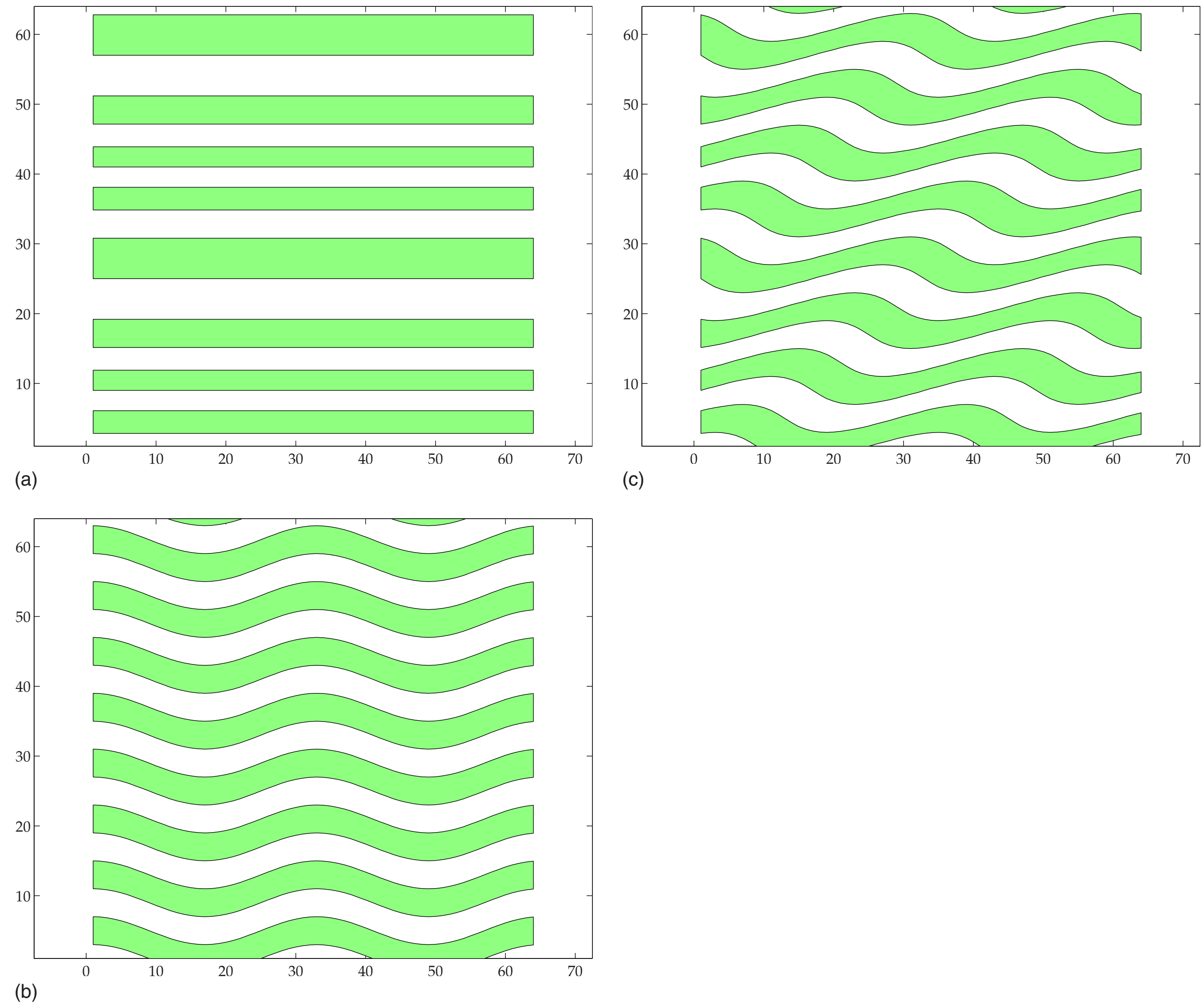

FIG. 6. (Color online) Perturbations with different orientations to the layer normal direction. Layer compression mode with $\theta=0$ (a), bending mode with $\theta=(\pi/2)$ (b), and oblique mode with $\theta=(\pi/4)$ (c).

tative behavior of the second sound speed is correctly reproduced in the simulations, and there is good quantitative agreement.

III. CONCLUSIONS

In the present analysis, a systematic framework for obtaining the macroscopic parameters (layer bending and compression moduli, permeation constant) from a mesoscale description (in terms of the concentration fields for the hydrophilic and hydrophobic domains) has been proposed for an ordered lamellar fluid. Although the present analysis is restricted to a symmetric lamellar phase in which the volume fractions of the hydrophilic and hydrophobic parts are equal, this can easily be extended to an asymmetric lamellar phase. This enables us to adjust the parameters in the mesoscale description in order to obtain consistency with both molecular level and macroscale descriptions, as discussed a little later.

At equilibrium, the solution for the concentration field from the mesoscale description was obtained as a function of the parameters r and k in the free energy functional (1). The parameter k provides the wave number for the concentration modulation, and $(2\pi/k)$ is the layer spacing. It was shown that the concentration profile is close to a sine wave for $r \gg 1$. In the limit $r \ll 1$, the interfaces between the hydrophilic and hydrophobic layers are sharp, and the profile has a series of alternating step functions of positive and negative signs. It was shown, analytically, that the interface thickness for the step function scales as $(r^{1/4}/k)$ in the limit $r \ll 1$. The concentration profiles, as well as the amplitudes of the higher harmonics in the expansion for the concentration field, were verified using LBM simulations. The sine profile in the limit $r \gg 1$ is relevant to surfactant systems where there is a large degree of diffusion and interpenetration between the oil and water layers, especially at high temperatures. It is also appropriate for block copolymers in the weak segregation limit, where there is significant interpenetration between the two blocks. The step profile in the limit $r \ll 1$ is applicable for stiff bilayers where there is no significant penetration in the layer normal direction and also to block copolymers in the strong segregation limit. Therefore, from the concentration

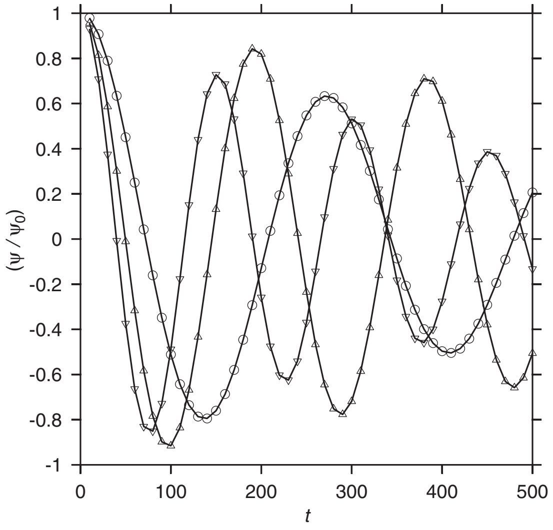

FIG. 7. Relaxation of perturbations with orientation angle with respect to the layer normal of $\theta=(\pi/6)$ (○), $\theta=(\pi/4)$ (△), and $\theta=(\pi/3)$ (∇).

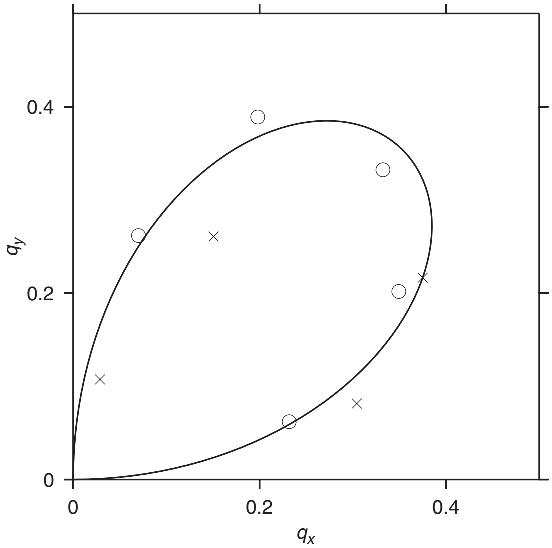

FIG. 8. Polar plot of the ratio $(c_s/\sqrt{B/\rho})$ which is the distance from the origin, as a function of the orientation of the wave vector from the vertical, which is the polar angle θ calculated with respect to the vertical. Here, c_s is the second sound speed (46). The line is the theoretical result Eq. (46), the circles are the simulation results with $r=100$ in the free energy functional (1), while the crosses are the results with $r=0.001$ in the free energy functional (1).

modulation obtained in simulations or from NMR studies, it is possible to obtain the parameters r and g for the zero tension state.

In order to analyze the energetics of the system, a small layer displacement u was imposed on the equilibrium concentration profile, and the free energy was reconstructed in terms of u and its derivatives in the limit where the scale for variation of u is large compared to the layer spacing. It was found that the resulting free energy functional has the same form as the lowest order (quadratic) approximation for the free energy (6) based on symmetry considerations alone. This enabled us to obtain quantitative results for the layer bending and compression moduli in terms of the parameters in the free energy functional (1). It was found that all the moduli are proportional to the energy scale A in the free energy functional (1). An interesting finding is that the surface tension is not zero when the parameter g is set equal to zero on the free energy functional (1), and it is necessary to set g equal to a negative value to reach the zero tension state.

The dynamical equations for the layer-displacement field were obtained by superposing a small displacement u on the concentration field, and then assuming that the length scale for the variation in the layer-displacement field is large compared to the layer spacing. The equations for the concentration field are the usual model-H equations. It was shown that the equations for the concentration field reduce to a permeation equation for the flow normal to the layers, in which the relative velocity between the fluid and the layers is given proportional to the force density (pressure gradient) in this direction (Darcy law). An explicit relationship was derived between the permeation constant and the Onsager coefficient in the equation for the concentration field; it is interesting to note that the permeation constant and the Onsager coefficient have the same units for this case. The mesoscale fluid momentum equation was also found to reduce to the usual Navier–Stokes equations, in which the momentum equation contains an additional force density due to the layer bending and compression.

The dispersion relations for the perturbations to the layer-displacement field were determined using a linear stability calculation. It was found that the decay of fluctuations is diffusive when perturbations are imposed along or perpendicular to the layers for the zero tension case; however, there are propagating modes when the perturbation is neither along nor perpendicular to the layers. The decay rates of the perturbations are found to be related to the layer bending and compression moduli, as well as to the fluid viscosity. Both the diffusive and the propagating behavior were recovered from the mesoscale LBM simulations for the concentration field.

The present analysis provides a framework for relating the mesoscale description in terms of the concentration field to the macroscopic description in terms of the layer-displacement field. We briefly discuss the extension of the present analysis in two ways; the first is the method for obtaining the mesoscale parameters from a microscopic (molecular dynamics) simulation and the second is a method for embedding the layer-displacement field into a macroscopic fluid dynamics simulation.

Due to computational constraints, actual molecular dynamics simulations[18] are restricted to a single bilayer in a fluid, and they do not simulate an actual lamellar phase. However, it should be noted that actual simulations are also carried out with periodic boundary conditions in all directions. So what is simulated is actually a multilayered system, in which each periodic cell contains one layer. This indicates that single layer simulations with periodic boundary conditions are actually lamellar phase simulations, in which the total layer spacing (wavelength of the concentration modulation) is equal to the box size in the direction perpendicular to the layers. However, it is important to note that due to finite box size, there is an upper limit on the wavelength of the fluctuations in the system. Subject to this limitation, the

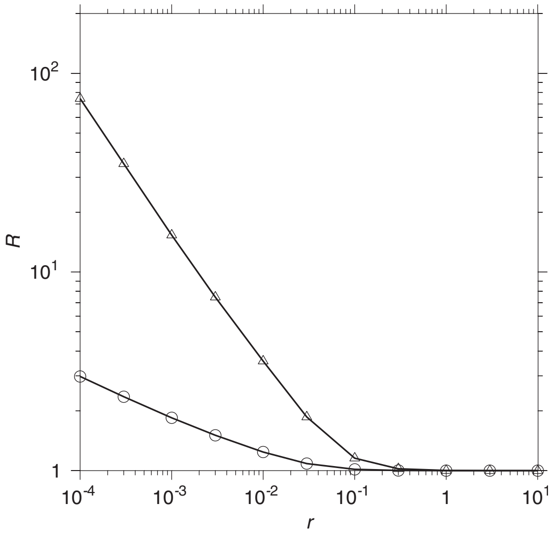

FIG. 9. The measures R_1 from Eq. (47) (○) and R_2 from Eq. (48) (△) as a function of r for the tensionless state.

properties of the lamellar phase can be extracted from simulations carried out with a single bilayer with periodic boundary conditions in the direction perpendicular to the bilayers.

In a microscopic simulation, one typically has access to the positions and momenta of all the molecules. The concentration profiles for the hydrophilic and hydrophobic parts can be obtained by averaging over time. From this, the parameters r and g can be determined for the tensionless state of the membrane. An intuitive method to fix the parameter r is to generate profiles for different values of r and then examine which is closest to the profile generated in simulations. A more quantitative method can be devised by realizing that the interface profile becomes more steplike as the parameter r decreases, and therefore the maximum gradient in the concentration field (at the point where the concentration goes through zero) becomes larger as r decreases. It is possible to get a measure of the increase in the gradient using, for example, the integral of the square of the gradient over one concentration wave,

$$R_1 = \frac{\int_0^L dz (d\psi/dz)^2}{k^2 \int_0^L dz \psi^2}. \tag{46}$$

The variation in R_1 with the parameter r is shown in Fig. 9 for the tensionless state. It is observed that there is a numerically small variation in R_1 when $r \ll 1$; theoretically, to within logarithmic factors, it can be shown that $R_1 \propto r^{-1/4}$ for $r \ll 1$. Since the power law dependence is very weak, it may not be possible to obtain numerically accurate results for this concentration profile. An alternative is to use the square of the second derivative as the measure

$$R_2 = \frac{\int_0^L dz (d^2\psi/dz^2)^2}{k^4 \int_0^L dz \psi^2}. \tag{47}$$

As shown in Fig. 9, R_2 shows a larger variation with r in the limit $r \ll 1$; theoretically, we would expect $R_2 \propto r^{-3/4}$ in the limit $r \ll 1$. However, it may be more difficult to obtain R_2 in simulations due to the larger errors incurred upon taking a higher derivative.

The energy scale A in the free energy functional (1) can be determined from either the compression or the bending modulus. It is most convenient to determine the bending modulus in fluctuations from the height-height correlation function at equilibrium. In this method, a single monolayer or bilayer membrane is simulated in a periodic box; the box size is suitably fixed in order to obtain the correct layer spacing. The membrane is considered to be flat and aligned along the x-y plane in the base state, and the fluctuations in the height of the membrane in the z direction, $h(x,y)$, are measured. The change in the free energy due to the height fluctuations is written as an integral of the form

$$F[u] = F_0 + \int dA \left(\frac{K_A (h_{xx} + h_{yy})^2}{2} \right), \tag{48}$$

where K_A is the bending modulus and the subscripts represent derivatives with respect to the spatial coordinates. The height coordinate is expressed in terms of its Fourier modes in the x and y coordinates,

$$h(\mathbf{k}) = \int dx \int dy \, \exp(\imath k_x x + \imath k_y y) h(x,y). \tag{49}$$

This is inserted into the free energy functional (7), and we use the equipartition condition that the energy in each Fourier mode is $(T/2)$ (where T is the product of the Boltzmann constant and the temperature), we obtain the equilibrium height-height correlation function as

$$\langle h(\mathbf{k}) h(-\mathbf{k}) \rangle = \frac{T}{A_m (K_A (k_x^2 + k_y^2)^2)}, \tag{50}$$

where A_m is the total membrane area. This height-height correlation function can be measured in simulations as a function of the wave number, and the layer bending modulus can be obtained in the long wave limit $(k_x, k_y) \to 0$. Note that as defined, the bending modulus K_A has dimensions of energy.

Apart from the fluid viscosity, there is only one dynamical parameter which enters into the description, which is the permeation constant which enters into the equation for the normal displacement field (28). This permeation constant is always between 1 and 1.5 times the Onsager coefficient in the dynamical equation (24), and therefore both of these can be determined simultaneously. The permeation constant can be determined from simulations,[18] where the effective potential for the transfer of a water molecule through the bilayer is analyzed. The permeation constant has two parts, one of which is the diffusion coefficient of water through the bilayer, while the second is the partition coefficient of water between the aqueous and organic phases. The diffusion coefficient of water through the bilayer is calculated in simulations[18] for a DPPC (dipalmitoylphosphatidylcholine) bilayer and is found to be of the order of $D \sim 10^{-8}\ \mathrm{m^2/s}$. The partition coefficient is more difficult to evaluate, but by taking the ratio of the permeation constant and the diffusion constant, we obtain a value of about $P_c \sim 10^{-3}$ for the partition of water between the aqueous and organic phases. Therefore, we assume an effective diffusion coefficient of

10^{-11} m^2/s. If we look at Eq. (32), for example, we can infer that the Onsager coefficient is related to the diffusion coefficient by $D=A\Gamma$. Therefore, the Onsager coefficient Γ can be estimated as 2.8×10^{-20} m^3 s/kg.

The thermodynamic dimensionless parameter that enters into the description is the ratio of the energy scale A and the thermal energy kT. At room temperature, $kT\sim 4\times 10^{-21}$ J. In order to compare the energy parameter A with the thermal energy, we can consider fluctuation perturbations on the smallest scale, which is the layer spacing, $\lambda\sim 10$ nm. A dimensionless number can be constructed as

$$\frac{A\lambda^3}{kT}\sim 3\times 10^3. \tag{51}$$

Therefore, thermal fluctuations are not important even for perturbations on the order of the lamellar spacing and can certainly be neglected for perturbations with a larger wavelength. The dimensionless parameter which enters into the dynamical description is the ratio of convection and diffusion.

In the fluid dynamical description, the only parameter that enters into the problem is the Reynolds number, (UL/ν) or $(\dot{\gamma}L^2/\nu)$, where U and $\dot{\gamma}$ are the velocity and the strain rate. We assume that $U\ll c_s$, where c_s is the speed of sound, so that the Mach number does not enter into the problem. It is not necessary to set c_s equal to the actual speed of sound, only to maintain it a large number (10^3) times the flow velocity. From the kinematic viscosity ν for the system, we can determine the relaxation time for momentum fluctuations from the relation $\nu=c_s^2(2\tau_1-1)/6$. The diffusion coefficient can be used to determine the second relaxation time $D=c_s^2(\tau_2-1/2)$.

If the viscosity of the fluid is considered to be 10^{-3} kg/m/s (the viscosity of water), then the kinematic viscosity is $\nu\sim 10^{-6}$ m^2/s. From the viscosity and the effective diffusion coefficient, we can obtain the Schmidt number as

$$Sc=\frac{\nu}{D}\sim 10^5. \tag{52}$$

For fluids of higher viscosity, the Schmidt number is likely to be even higher. The dynamical dimensionless numbers are the Reynolds number, which is the ratio of inertia and viscosity, and the Peclet number, the ratio of convection and diffusion. The Reynolds number is typically small. For example, if we assume a strain rate of $\dot{\gamma}\sim 1$ s^{-1} and a length scale of $L\sim 1$ mm, a fluid with the viscosity of water will have a Reynolds number $\mathrm{Re}\sim(\dot{\gamma}L^2/\nu)\sim 1$, while a fluid with a higher viscosity will have a much lower Reynolds number. This implies that the inertial terms can be neglected in the fluid momentum equation. However, the Peclet number $\mathrm{Pe}=(\dot{\gamma}L^2/D)\sim 10^5$ is typically large because the diffusion coefficient is small compared to the kinematic viscosity. Therefore, the convective effects could dominate in the fluid momentum conservation equation.

The scaling of the conservation equations for the fluid momentum and the concentration field depend on whether the lamellar phase is freely evolving or whether there is an imposed shear. In the case of an imposed shear, the appropriate time scale in the momentum equation is the inverse of the strain rate $\dot{\gamma}^{-1}$, while the length scale is the size of the domain, L. If there were no flow, the system would be at equilibrium (in the absence of kinetic constraints), and the chemical potential $\mu_c=(\delta F/\delta\psi)$ would be zero. Here, we use the superscript c to distinguish the chemical potential from the viscosity μ. In the presence of flow, there is a nonzero contribution to the chemical potential which can be estimated from the momentum equation (24). In order to express the equations in dimensionless form, it is convenient to work with a dimensionless chemical potential, defined as $\mu_c^*=(\mu_c/A)$. In the momentum conservation equation, the viscous term can be estimated as $(\nu\dot{\gamma}/L)$, while the term proportional to the concentration gradient is $(A\mu^*/\rho\lambda)$, where λ is the lamellar spacing. A balance between these provides the magnitude of the chemical potential as $\mu^*=(\nu\rho\dot{\gamma}\lambda/LA)$. In the concentration equation, the convective term can be estimated as $(\dot{\gamma}L/\lambda)$, since the velocity scales as $\dot{\gamma}L$ and the length scale for concentration variations is λ. The diffusive term scales as $(\Gamma A\mu^*/\lambda^2)$. The ratio of the diffusive and convective terms is given by $(\Gamma A\mu^*/L\lambda\dot{\gamma})$, which is proportional to $(\rho\nu\Gamma/L^2)$. This is small compared to 1 for lengths large compared to the layer spacing, and so the diffusion term in the concentration equation can be neglected in comparison to the convective transport terms.

If the Reynolds number is small, then the inertial terms in the momentum conservation equation can be neglected in comparison to the viscous terms. The concentration and momentum equations then become

$$\nabla\cdot\mathbf{v}=0, \tag{53}$$

$$-\nabla p+\mu\nabla^2\mathbf{v}+f_z=0, \tag{54}$$

$$\left(\frac{\partial u}{\partial t}-v_z\right)=Pf_z. \tag{55}$$

In the equation for the displacement field, the permeability P is very nearly equal to the Onsager coefficient Γ, while $f_z\sim Bu_{zz}$ if there is layer compression. The product $PB\sim D$, where D is the diffusion coefficient.

The macroscopic length scale in the problem has to be chosen with care, since the choice will affect the scaling of the bending and compression terms in the layer-displacement equation. Assume L_n and L_t are the length scales for the variation in the layer-displacement field in the directions normal and tangential to the layers. Then for the bending and compression terms in the force density (27) to be of equal magnitude, we require that $(Bu/L_n^2)\sim(Ku/L_t^4)$. For $r\gg 1$ where the concentration profile is close to a sine wave, the layer bending and compression moduli are related as $B=K\lambda^2$, where λ is the layer spacing. In this case, a balance between the bending and compression terms in the force density f_z shows that $(L_n/L_t)\sim(L_t/\lambda)$. This is an indication that for a system near equilibrium, the propagation of a disturbance in the direction normal to the layers takes place over a much larger distance than the extent of the disturbance parallel to the layers. Therefore, it is necessary to consider, separately, the length scales in the two directions.

First, we consider the case where the macroscopic scale L is the length scale for the coordinate z along the direction of the layer normal and define the scaled distance as $z^* = (z/L)$. The scaling of the layer-displacement field needs to be carried out carefully. The linear analysis can be used only if the strain u_z is, at most, $O(1)$. Therefore, the layer-displacement field has to be scaled by the macroscopic length scale L, so we define $u^* = (u/L)$. We obtain the time scale by balancing the concentration-dependent force in the momentum equation. In this case, we find that the displacement field u is related to the velocity field $\mathbf{v}$ by $\mathbf{v} \sim (B/\mu)u$. Therefore, the appropriate time scale in the problem is (μ/B), and the time can be scaled by this time scale. In dimensionless terms, the momentum conservation equation reduces to

$$-\nabla^* p^* + \nabla^{*2}\mathbf{v}^* + f_z^* = 0, \tag{56}$$

where the dimensionless force density $f_z^* = (f_z L/B)$, and the dimensionless pressure $p^* = (p/B)$. The scaled equation for the concentration field is

$$\left(\frac{\partial u^*}{\partial t^*} - v_z^*\right) = \left(\frac{\mu P}{L^2}\right) f_z^*. \tag{57}$$

Since the coefficient of the term on the right side is usually small, it can be neglected in the leading approximation.

Alternatively, one can consider a situation where the macroscopic scale L is the length scale for layer bending. In this case, the length scale for layer compression is (L^2/λ), where λ is the layer spacing, as shown earlier. Therefore, the layer compression over lengths comparable to L is negligible. The force density f_z can be estimated as $f_z = (Ku/L^4)$, where K is the bending constant. If we use this for scaling the momentum conservation equation, as before, then the appropriate time scale is $(\mu L^2/K)$ instead of (μ/B). With this, the momentum conservation equation assumes the same form as Eq. (56), and the permeation equation is of the same form as (57), although the scaled force density is now defined as $f_z^* = (f_z L^3/B)$ and $p^* = (pL^2/K)$. Therefore, in both cases, the scaled equations for the fluid momentum and the layer-displacement field have the same form. In both cases, the relative magnitude of the forcing term in the permeation equation is proportional to the dimensionless number $(\mu P/L^2)$, which is small for typical applications.

We next turn to a macroscale simulation of the dynamics of lyotropic liquid crystal media, which requires the solution of the layer-displacement equation (55) in conjunction with the fluid mass and momentum equations, (53) and (54). First, it is necessary to define two additional fields, the layer spacing field w and the layer normal field $\mathbf{n}$, where $\mathbf{n}$ is a unit normal. It is more convenient to define the layer spacing field as the ratio between the layer spacing and the equilibrium layer spacing in the absence of stresses, so that this is a dimensionless field. These could both be combined into a single vector layer-displacement field $\mathbf{w} = w\mathbf{n}$, but we will write equations for these two separately. It is necessary to resolve the local velocity fields into two components, one along the normal to the layers and the other tangential to the layers, where the unit normal to the layers is a function of position. The velocity field is resolved into two components,

$$\begin{aligned} v_n &= \mathbf{n} \cdot \mathbf{v}, \\ \mathbf{v}_t &= (\mathbf{I} - \mathbf{nn}) \cdot \mathbf{v}, \end{aligned} \tag{58}$$

where v_n and $\mathbf{v}_t$ are the components of the velocity normal and tangential to the layers.

In addition to the fluid velocity field, it is also necessary to define a velocity field for the surfactants, which could be different from the fluid velocity field due to permeation. It is variations in the surfactant displacement that leads to layer compression and bending. We define $\mathbf{v}_s$ as the surfactant velocity field. This can be resolved into components along the local unit normal and along the plane of the layers,

$$\begin{aligned} v_{sn} &= \mathbf{n} \cdot \mathbf{v}_s, \\ \mathbf{v}_{st} &= (\mathbf{I} - \mathbf{nn}) \cdot \mathbf{v}_s. \end{aligned} \tag{59}$$

The evolution of the unit normal field is determined from kinematic conditions. The substantial derivative for the unit normal field is related to the gradient in the normal component of the fluid velocity along the direction tangential to the layers,

$$\frac{D\mathbf{n}}{Dt} = (\mathbf{I} - \mathbf{nn}) \cdot \nabla v_{sn}. \tag{60}$$

Here, the substantial derivative is defined as the derivative translating and rotating with the local fluid element,

$$\frac{D}{Dt} = \frac{\partial}{\partial t} + \mathbf{v} \cdot \nabla. \tag{61}$$

Equation (60) ensures that the magnitude of the unit normal does not change with time, that is, $\mathbf{n} \cdot (D\mathbf{n}/Dt) = 0$. The change in the layer-displacement field is due to the variation of the velocity normal to the layers along the direction normal to the layers.

$$\frac{Dw}{Dt} = w\mathbf{n} \cdot \nabla v_{sn}. \tag{62}$$

This equation indicates that the layer spacing increases when the normal velocity increases with distance along the unit normal, and it decreases when the normal velocity decreases with distance along the unit normal.

In order to obtain the force density due to layer compression and bending, it is first necessary to define the compression and bending terms in terms of the layer spacing and unit normal fields. The compression of the layers results in a variation in the layer spacing field in the direction of the unit normal, acting in the direction of the unit normal. Therefore, the compression stress can be written as

$$f_n^{\text{bending}} = B\mathbf{n} \cdot \nabla w. \tag{63}$$

The force density due to curvature is proportional to the Laplacian of the radius of curvature along the plane tangential to the unit normal,

$$f_n^{\text{curvature}} = K(\nabla^2 - \mathbf{nn}:\nabla\nabla)(\nabla \cdot \mathbf{n}). \tag{64}$$

The total force density can now be written as the sum of these three components,

$$f_n = B\mathbf{n}\cdot\nabla w + K(\nabla^2 - \mathbf{nn}:\nabla\nabla)(\nabla\cdot\mathbf{n}). \tag{65}$$

Next, we turn to the dynamical equations. The permeation equation for the normal component of the velocity of the bilayer can be written as

$$(v_{sn} - \mathbf{n}\cdot\mathbf{v}) = Pf_n, \tag{66}$$

where $\mathbf{n}\cdot\mathbf{v}$ is the velocity along the unit normal to the bilayers. In the case the dimensionless number $(\mu P/L^2)$ is small, the term on the right side of Eq. (66) can be neglected, and we set the bilayer velocity equal to the fluid velocity. The momentum equation for the fluid is

$$\rho\left(\frac{\partial\mathbf{v}}{\partial t} + \mathbf{v}\cdot\nabla\mathbf{v}\right) = -\nabla p + \mu\nabla^2\mathbf{v} + \mathbf{n}f_n. \tag{67}$$

Equations (60), (62), (66), and (67) form a complete set of equations for determining the layer spacing, unit normal, and fluid velocity fields at all points in the flow.

The authors would like to thank Professor K. G. Ayappa, Professor P. Maiti, and Professor Sriram Ramaswamy for interesting discussions. Financial support from Proctor & Gamble, USA, is gratefully acknowledged.

APPENDIX: SIMULATION TECHNIQUE

In order to compare the analytical results with the simulations, we use the LB simulation technique which is a mesoscopic simulation technique. Here, particle positions are discretized on a lattice, and the velocity vectors are chosen such that a particle traverses from one node to the neighboring node in unit time step. Rather than follow particles, it is more convenient to track the distribution function for the velocities in the discrete directions. The density and momenta are conserved at each step of the simulation, and it can be shown that this microscopic model correctly reproduces the Navier–Stokes directions for the mean velocity field on length scales large compared to the lattice spacing. This is different from conventional finite element or finite difference techniques where the governing partial differential equations for the fluid are not explicitly solved in the simulations. We first discuss the application of the LB technique to a simple fluid and describe the extension to a mesoscopically ordered lamellar fluid.

In the simulation, the distribution function is defined at the nodes of a discrete lattice. The distribution function is a function of the lattice position and a set of discrete velocities along the directions joining lattice points which are chosen such that transport from one node to the next along the lattice direction takes place in one time step. The distribution function $f_a(\mathbf{x},t)$ provides the probability of finding a particle at the lattice position $\mathbf{x}$ with velocity in the $\mathbf{e}_a$. In our simulations, the D2Q9 formulation is used in two dimensions, where each node is connected to the neighboring nodes along the coordinate directions and along the diagonals in a square lattice. The distribution function in this case is a function of nine velocities, eight of which are along the links between lattice nodes and the ninth velocity is set to zero. The macroscopic properties of the fluid, such as the density, mean velocity, and stress are related to the velocity moments of the distribution function in a manner similar to that in the kinetic theory of gases,[19]

$$\begin{aligned}
&\sum_a f_a = \rho,\\
&\sum_a f_a e_{a\alpha} = \rho u_\alpha,\\
&\sum_a \frac{1}{2} f_a(\mathbf{e}_a - \mathbf{u}) = \rho E,\\
&\sum_a f_a e_{a\alpha} e_{a\beta} = \rho u_\alpha u_\beta - \rho C_s^2\delta_{\alpha\beta} + \sigma_{\alpha\beta},
\end{aligned} \tag{A1}$$

where $\mathbf{u}$ is the mean velocity, E is the internal energy of the gas due to molecular motion, C_s is the speed of sound, and $\sigma_{\alpha\beta}$ is an additional contribution to the stress tensor due to concentration variations which is discussed below. Note that the indicial notation is used to represent vectors and tensors, where Greek subscripts denote the directions of a vector, and repeated indices represent a dot product.

The mesoscopic model for the variation in the distribution function in the LB method consists of two steps. In the "streaming" step, the particles with velocity $\mathbf{e}_a$ are transferred from their present node $\mathbf{x}$ to the adjacent node $\mathbf{x}+\mathbf{e}_a$ in one time step,

$$f_a(\mathbf{x}+\mathbf{e}_a, t+1) = f_a(\mathbf{x},t). \tag{A2}$$

In the "collision" step, all particles incident on a node after the streaming step are redistributed at the node according to a set of "collision rules." The process of streaming and collision can be written as

$$f_a(\mathbf{x}+\mathbf{e}_a, t+1) - f_a(\mathbf{x},t) = \Omega_a, \tag{A3}$$

where Ω_a is the collision matrix (analogous to the collision integral in the Boltzmann equation). Equation (A3) is called the Lattice Boltzmann equation (LBE), which is the discrete version of the Boltzmann equation in the kinetic theory of gases. It is known that the LBE also provides the same macroscopic equations for the macroscopic density and mean velocity in a gas as the Boltzmann equation.

The collision rules are chosen such that mass, momentum, and energy are conserved at every collision. In order to simplify the solution procedure for gases close to equilibrium, the single relaxation time approximation of the collision integral was proposed by Bhatnagar *et al.*[20] [BGK (Bhatnagar-Gross-Krook) approximation],

$$\frac{d_c f_a}{dt} = \frac{-(f_a - f_a^{\mathrm{eq}})}{\tau}, \tag{A4}$$

where f_a^{eq} is the equilibrium distribution under the local conditions of temperature and pressure and τ is the relaxation time constant. This approximation has been adapted to the LBE, so that the complete form of this equation is[21]

$$f_a(\mathbf{x}+\mathbf{e}_a,t+1)-f_a(\mathbf{x},t)=\frac{-[f_a(\mathbf{x},t)-f_a^{\mathrm{eq}}(\mathbf{x},t)]}{\tau}, \tag{A5}$$

where τ is the relaxation time in the LBE. The equilibrium distribution is assumed to be of a simple form

$$f_a^{eq}(\mathbf{u})=\rho[A_1+A_2(\mathbf{u}\cdot\mathbf{e}_a)+A_3(\mathbf{u}\cdot\mathbf{e}_a)^2+A_4\mathbf{u}^2 + (\mathbf{G}:\mathbf{e_a}\mathbf{e_a})], \tag{A6}$$

where the constants A_1-A_4 are chosen such that the equilibrium distribution satisfies the conditions[22]

$$\begin{aligned}&\sum_a f_a^{\mathrm{eq}}=\rho,\\ &\sum_a f_a^{\mathrm{eq}}e_{a\alpha}=\rho u_\alpha,\\ &\sum_a f_a^{\mathrm{eq}}e_{a\alpha}e_{a\beta}=\rho C_s^2\delta_{\alpha\beta}+\rho u_\alpha u_\beta,\\ &\sum_a f_a^{\mathrm{eq}}e_{a\alpha}e_{a\beta}e_{a\gamma}=\text{to be isotropic},\end{aligned} \tag{A7}$$

where ρC_s^2 is the pressure and, C_s the speed of sound, is $(1/3)^{1/2}$ in this model. It can be shown that the above scheme, using a nine velocity model in two dimensions, correctly reproduces the dynamics of a Newtonian fluids with kinematic viscosity $\nu=(2\tau-1)/6$ at length scales large compared to the lattice spacing. The additional contribution to the equilibrium stress tensor due to concentration fluctuations is incorporated in the tensor **G**, and this is discussed below.

In order to obtain lamellar phases, it is necessary to prescribe an additional concentration field ψ which locates the positions of the lamellae, and it can be assumed without loss of generality that the lamellae are located at positions where the value of this function is zero. The appropriate equilibrium free energy is of the form

$$F[\psi]=A\int dV\left(-\frac{\psi^2}{2}+\frac{\psi^4}{4}+\frac{r}{4k^2}((\nabla^2+k^2)\psi)^2 + \frac{g}{2k^2}(\nabla\psi)^2\right), \tag{A8}$$

where the concentration field ψ is assumed to be dimensionless and A has dimensions of an energy density (energy per unit volume). The first three terms on the right side correspond to the usual Landau–Ginzburg free energy and favor phase separation into two domains of concentration $\psi=\pm1$. The third term on the right side favors a lamellar phase because it provides an energy penalty when the wavelength of the concentration field is not equal to $(2\pi/k)$. The nature of the concentration field modulation in the lamellar phase (sine wave or square wave) is determined by the dimensionless parameter r in Eq. (A8); this is discussed in detail a little later.

The concentration field is incorporated in the simulation by defining an additional distribution $g_a(\mathbf{x},t)$, which is related to the macroscopic variables by

$$\begin{aligned}&\sum_a g_a=\psi,\\ &\sum_a g_a e_{a\alpha}=\psi u_\alpha.\end{aligned} \tag{A9}$$

The evolution equation for the distribution $g_a(\mathbf{x},t)$ is similar to that for the distribution function for the total density $f_a(\mathbf{x},t)$ (single relaxation time approximation),

$$g_a(\mathbf{x}+\mathbf{e}_a,t+1)-g_a(\mathbf{x},t)=\frac{-[g_a(\mathbf{x},t)-g_a^{\mathrm{eq}}(\mathbf{x},t)]}{\tau_g}, \tag{A10}$$

where τ_g is the relaxation time for the concentration field. The equilibrium distribution g_a^{eq} is defined so that the resulting continuum equations describe the dynamics of a binary liquid mixture. A suitable choice is[6,7]

$$\begin{aligned}&\sum_a g_a^{\mathrm{eq}}=\psi,\\ &\sum_a g_a^{\mathrm{eq}}e_{a\alpha}=\psi u_\alpha,\\ &\sum_a g_a^{\mathrm{eq}}e_{a\alpha}e_{a\beta}=\Gamma\Delta\mu\delta_{\alpha\beta}+\psi u_\alpha u_\beta,\\ &\sum_a g_a^{\mathrm{eq}}e_{a\alpha}e_{a\beta}e_{a\gamma}=\text{to be isotropic},\end{aligned} \tag{A11}$$

where Γ is the mobility and $\Delta\mu$ is the chemical potential difference between the two components,

$$\Delta\mu=\frac{\delta F}{\delta\psi}, \tag{A12}$$

$$=\frac{dF}{d\psi}-\partial_\alpha\frac{dF}{d(\partial_\alpha\psi)}+\nabla^2\frac{dF}{d(\nabla^2\psi)}. \tag{A13}$$

Note that in expanding functional derivatives, the symbol d is used to denote partial derivatives of the free energy with respect to ψ, $\partial_\alpha\psi$, and $\nabla^2\psi$ in order to distinguish this from the spatial derivatives. A general form of the equilibrium distribution is

$$g_a^{\mathrm{eq}}(\mathbf{u})=\psi[B_1+B_2(\mathbf{u}\cdot\mathbf{e}_a)+B_3(\mathbf{u}\cdot\mathbf{e}_a)^2+B_4\mathbf{u}^2] \tag{A14}$$

for a discrete set of velocities.[6,7] If necessary, more terms could be added to the above expansion. The nonideal part of the equilibrium pressure tensor is incorporated using the tensor $G_{\alpha\beta}$. The introduction of the $G_{\alpha\beta}$ term in f_a^{eq} distribution function always guarantees the conservation of mass and momentum.

It can be shown that the above scheme correctly reproduces the macroscopic mass and momentum conservation equations for the fluid,

$$\partial_t\rho+\partial_\alpha(\rho u_\alpha)=0, \tag{A15}$$

$$\partial_t(\rho u_\alpha)+\partial_\beta(\rho u_\alpha u_\beta)=-\partial_\alpha p+\nu\partial_\beta^2 u_\alpha+\partial_\beta\sigma_{\alpha\beta}, \tag{A16}$$

where the kinematic viscosity $\nu=(2\tau-1)/6$ is related to the relaxation time for the fluid density distribution and the pressure $p=\rho C_s^2$, where C_s is the speed of sound.

The last term on the right side of the Eq. (A16) is the additional force density caused by concentration variations. In the model-H formulation, for incompressible binary fluids, the momentum equation is given by

$$\rho\left(\frac{\partial v_\alpha}{\partial t}+v_\beta\partial_\beta v_\alpha\right)=-\partial_\alpha p+\mu\partial_\beta^2 v_\alpha+(\partial_\alpha\psi)\frac{\delta F}{\delta\psi}. \tag{A17}$$

The last term on the right side of the above equation is the complement of the convective term in the concentration equation and is obtained using Poisson-bracket relations. Therefore, the concentration-dependent stress has to satisfy the condition

$$\begin{aligned}\partial_\beta\sigma_{\alpha\beta}=(\partial_\alpha\psi)\frac{\delta F}{\delta\psi}=\partial_\alpha&\left(-\frac{\psi^2}{2}+\frac{\psi^4}{4}+\frac{r\psi^2}{2}\right)\\&-(g/k^2)(\partial_\alpha\psi)(\partial_\beta^2\psi)\\&+(r/k^4)(\partial_\alpha\psi)(\nabla^4\psi+2k^2\nabla^2\psi).\end{aligned} \tag{A18}$$

The first term on the right of the above equation can be combined with the gradient of the fluid pressure, which is determined by the incompressibility condition for the fluid. The last term on the right provides a nonzero contribution to the deviatoric stress, and the stress tensor corresponding to this is determined by postulating a stress tensor of the form

$$\begin{aligned}\sigma_{\alpha\beta}=&\left(-\frac{\psi^2}{2}+\frac{\psi^4}{4}+\frac{r\psi^2}{2}\right)\delta_{\alpha\beta}+\frac{2r}{k^2}(\partial_\alpha\psi)(\partial_\beta\psi)\\&+\frac{r}{k^4}((\partial_\alpha\psi)(\partial_\beta\nabla^2\psi)+(\partial_\beta\psi)(\partial_\alpha\nabla^2\psi))\\&-\frac{g}{k^2}(\partial_\alpha\psi\partial_\beta\psi),\end{aligned} \tag{A19}$$

where the isotropic "pressure" p' is of the form

$$\begin{aligned}p'=&-\frac{\psi^2}{2}+\frac{\psi^4}{4}+\frac{r\psi^2}{2k^4}-\frac{r}{k^2}(\partial_\alpha\psi)^2-\frac{r}{k^4}(\partial_\beta\psi)(\partial_\beta\nabla^2\psi)\\&-\frac{r}{2k^4}(\nabla^2\psi)^2+\frac{g}{2k^2}(\nabla\psi)^2.\end{aligned} \tag{A20}$$

The macroscopic concentration equation is

$$\partial_t\psi+\partial_\alpha(\psi u_\alpha)=\Gamma\partial_\beta^2(\Delta\mu), \tag{A21}$$

where $\Gamma=(\tau_g-(1/2))$.

In the numerical procedure, the distribution function is evolved in time in accordance with the above rules on a square lattice starting with a set of initial concentration and velocity values. The fluid velocity is kept small compared to the speed of sound in order to approximate an incompressible flow. The evolution of the distribution function for the total density provides the mean velocity and stress, while the positions of the lamellae are determined from the contours of zero concentration. The code has been validated for Couette and Poiseuille flow in a channel and for the spinodal decomposition in a binary fluid, and the simulation results are in agreement with analytical solutions for these cases, thereby validating the numerical procedure.

[1] R. G. Larson, Rheol. Acta **32**, 245 (1993).
[2] H. A. Barnes, J. F. Sutton, and K. Walters, *An Introduction to Rheology* (Elsevier, Amsterdam, 1993).
[3] A. Xu, G. Gonnella, and A. Lamura, Phys. Rev. E **74**, 011505 (2006).
[4] F. Corberi, G. Gonnella, and A. Lamura, Phys. Rev. E **66**, 016114 (2002).
[5] G. Gonnella, E. Orlandini, and J. M. Yeomans, Phys. Rev. E **58**, 480 (1998).
[6] E. Orlandini, M. R. Swift, and J. Yeomans, Europhys. J. **32**, 463 (1995).
[7] V. Kumaran, S. K. Jariwala, and S. Hussain, Chem. Eng. Sci. **56**, 5663 (2001).
[8] S. Chen and G. D. Doolen, Annu. Rev. Fluid Mech. **30**, 329 (1998).
[9] F. S. Bates and G. H. Fredrickson, Annu. Rev. Phys. Chem. **41**, 525 (1990).
[10] L. Leibler, Macromolecules **13**, 1602 (1980).
[11] A. N. Semenov, Sov. Phys. JETP **61**, 733 (1985).
[12] G. Grinstein and R. A. Pelcovits, Phys. Rev. Lett. **47**, 856 (1981).
[13] O. Stenull, Phys. Rev. E **78**, 031704 (2008).
[14] G. Basappa, S. V. Kumaran, P. R. Nott, S. Ramaswamy, V. M. Naik, and D. Rout, Eur. Phys. J. B **12**, 269 (1999).
[15] M. Zapotocky, L. Ramos, P. Poulin, D. A. Weitz, and T. C. Lubensky, Science **283**, 209 (1999).
[16] M. Kleman, *Points, Lines and Walls in Anisotropic Fluids and Ordered Media* (Wiley, Chinchester, 1983).
[17] P. C. Hohenberg and B. I. Halperin, Rev. Mod. Phys. **49**, 435 (1977).
[18] S.-J. Marrink and H. J. C. Berendsen, J. Phys. Chem. **98**, 4155 (1994).
[19] J. O. Hirschfelder, C. F. Curtis, and R. B. Bird, *Molecular Theory of Gases* (Wiley, New York, 1954).
[20] P. L. Bhatnagar, E. P. Gross, and M. Krook, Phys. Rev. **94**, 511 (1954).
[21] M. R. Swift, E. Orlandini, W. R. Osborn, and J. M. Yeomans, Phys. Rev. E **54**, 5041 (1996).
[22] S. K. Jariwala, "Lattice Boltzmann simulation of the lamellar phase," ME thesis, Indian Institute of Science, 2000.